Extended Mermin Method for Calculating the Electron Inelastic Mean Free Path

B. Da,[1,*] H. Shinotsuka,[1,†] H. Yoshikawa,[1] Z. J. Ding,[2] and S. Tanuma[1]
[1]National Institute for Materials Science, 1-2-1 Sengen, Tsukuba, Ibaraki 305-0047, Japan
[2]Department of Physics, University of Science and Technology of China, 96 Jinzhai Road, Hefei, Anhui 230026, China
(Received 18 April 2014; revised manuscript received 3 June 2014; published 7 August 2014)

We propose an improved method for calculating electron inelastic mean free paths (IMFPs) in solids from experimental energy-loss functions based on the Mermin dielectric function. The "extended Mermin" method employs a nonlimited number of Mermin oscillators and allows negative oscillators to take into account not only electronic transitions, as is common in the traditional approaches, but also infrared transitions and inner shell electron excitations. The use of only Mermin oscillators naturally preserves two important sum rules when extending to infinite momentum transfer. Excellent agreement is found between calculated IMFPs for Cu and experimental measurements from elastic peak electron spectroscopy. Notably improved fits to the IMFPs derived from analyses of x-ray absorption fine structure measurements for Cu and Mo illustrate the importance of the contribution of infrared transitions in IMFP calculations at low energies.

DOI: 10.1103/PhysRevLett.113.063201 PACS numbers: 77.22.-d, 34.50.Bw, 72.10.-d

The electron inelastic mean free path (IMFP) is the average distance traveled between successive inelastic collisions by an electron moving with a particular energy in a given material [1]. It is an essential parameter for determination of surface sensitivity and quantitative analysis in electron-beam techniques such as x-ray photoelectron and Auger electron spectroscopy [2,3].

IMFPs are, however, difficult to determine experimentally, especially at energies below 200 eV [4–7]. Much effort has been devoted to IMFP measurements for various materials by use of elastic peak electron spectroscopy (EPES) [5–7]. This technique requires reference IMFP data, which strongly constrain its applicability, and variations of up to 20% between different measurements are common. Tanuma *et al.* [8] improved the EPES technique to wean it from its dependence on a reference IMFP. Although this refined approach can provide very reliable results at keV energies, it is still not appropriate for application at low energies, because of strong surface effects. Recently, another approach has been proposed to determine the IMFPs of Cu and Mo at energies below 120 eV by analysis of x-ray absorption fine structure (XAFS) [9,10], and this is expected to be more reliable than EPES for these energies. However, because of limitations of the theoretical model [11], it does not work for electron energies above 120 eV and so cannot be verified by comparison with the well-established results at keV energies from other experiments. Therefore, we can only hope to critically evaluate the XAFS technique by theoretical means.

One of the most popular algorithms for determining the IMFP in solids was proposed by Penn [12], in which the energy dependence of the energy-loss function (ELF) is obtained from experimental optical data for the material of interest and the dependence of the ELF on momentum transfer q is obtained from the Lindhard model dielectric function. The finite lifetimes of plasmons, however, are neglected in the Lindhard function, whereas it is well known that in real materials these excitations are damped. Mermin [13] derived an expression for the dielectric function $\varepsilon_M(q,\omega)$ that takes the plasmon lifetime into account and also preserves the local electron number. Recently, Denton *et al.* [14] modeled the momentum-dependent ELF using Mermin-type terms that explicitly include broadening effects at nonzero momentum transfer based on the Lindhard dielectric function. Introducing the ELF momentum dependence through the Mermin dielectric function provides a more natural extension of its wave number dependence and therefore should be a more realistic model for IMFP calculations.

Instead of directly using experimental optical ELFs, a component-based fit preprocessing is necessary for an externally determined optical ELF in the Mermin approach. The accuracy of the Mermin approach depends on the availability of ELF data at $q = 0$ that can be suitably fitted. This point, however, has been neglected, since regular fitting procedures are unable to model infrared transitions and inner shell electron excitations in optical ELFs with Mermin-type terms. The omission of these terms, especially the infrared transitions in the very low energy range, inevitably leads to errors in the calculated IMFPs, which become significant at energies below 10 eV because of the larger relative deviations by as much as a few times between fitted and original ELFs. Because of these errors in the fitted ELFs, the basis of the existing Mermin method is not entirely convincing. The IMFPs, especially below 200 eV, calculated with this approach in recent publications [15,16] remain discrepant from experimental data. Here we

propose an improved method for IMFP calculations from model ELFs that are obtained from curve fits with Drude functions including not only electronic transitions but also infrared transitions and inner shell excitations. In this way, we are able to make use of accurate Mermin ELFs obtained from fits to measured optical ELFs over a wide energy range.

To calculate IMFPs in the Mermin-model dielectric function approach, we fit the experimental ELF of a material in the optical limit ($q = 0$) by using a linear combination of Mermin-type ELFs or Drude functions,

$$\mathrm{Im}\left[\frac{-1}{\varepsilon(q=0,\omega)}\right] = \sum_{i=1}^{N} a_i \mathrm{Im}\left[\frac{-1}{\varepsilon_M(q=0,\omega;\omega_{pi},\gamma_i)}\right] = \sum_{i=1}^{N} \frac{\gamma_i \omega \omega_{pi}^2}{(\omega^2-\omega_{pi}^2)^2+\gamma_i^2\omega^2}, \quad (1)$$

with ε_M being the Mermin-type dielectric function [13]. The parameters a_i, ω_{pi}, and γ_i are the oscillator strength, energy, and width of the ith oscillator, respectively. We note that negative values of a_i are permitted in the fitting procedure.

Abril *et al.* [17,18] developed the MELF-GOS (Mermin-type ELFs with generalized oscillator strengths) model to treat experimental optical ELFs, which uses separate approaches for contributions to the ELF due to excitations from outer and inner shell electrons. We refer to this as the normal Mermin (NM) method. It employs only a small number of traditional oscillators, of order 1–10, to describe outer shell electron excitations in the optical ELF. It is very difficult to obtain satisfactory results with this procedure, even for valence electron or plasmon excitations, because one often sees a very sharp change in the ELF on the low-energy side due to the contribution of infrared transitions or, for nonmetallic materials, the band gap. In addition, Abril *et al.* used the GOS approach to describe excitations of inner shell electrons. It is worth mentioning that this NM method was once named "extended Mermin model" in de la Cruz and Yubero's work [19] in which they studied the influence of several model dielectric descriptions of the momentum-dependent ELF on the calculation IMFPs. To improve the quality of the Mermin approach, we have developed an extended Mermin (EM) model in which a modified oscillator scheme is adopted.

First, large numbers of extra oscillators were added to describe the contribution of infrared transitions and inner shell excitations. This, however, did not dramatically improve the fits with reasonable oscillator widths γ_i. To further improve the technique, some of the oscillator strengths a_i were allowed to take negative values during the fitting. These make a negative contribution to the ELF, but negative *total* ELFs are forbidden at any energy. The combination with positive oscillators can be used to accurately describe the sharp features around the band-gap energy or an inner shell excitation energy, thus avoiding the separate calculations for outer and inner shell excitations in the EM approach. Our procedure not only extends the traditional approach to infrared transitions and inner shell excitations simply and naturally but also results in a more accurate approximation to the optical ELF over the whole energy range.

Recently, Werner *et al.* [20] and Tahir *et al.* [21] obtained optical ELF data for Cu from experimental REELS spectra based on two separate deconvolution procedures, respectively. However, due to complicated electron-transport processes, the ELF is involved in a measured REELS spectrum in a more complex way other than simple convolutions [22]. Therefore, after comparing with transmission electron energy-loss measurements and verifying by sum rules, we employed ELFs obtained from optical measurements [23,24] as well as atomic photoabsorption data [25] for photon energies beyond the particular measurement range. Experimental optical ($q = 0$) ELFs for Cu [23–25] are compared with fitting results in Fig. 1. The dotted orange lines represent Abril *et al.*'s fit [17] with five Mermin-type ELFs used for Cu. The solid red lines show ELFs fitted with the EM method. We used 77 Mermin-type ELFs; of these, 37 negative oscillators were employed to significantly improve the accuracy of the approximation for sharp features in the ELFs. To visually demonstrate the importance of the negative-oscillator technique, their contributions are shown by blue and green lines to represent the contributions from positive and negative oscillators, respectively. Figure 1 reveals an excellent fit to the $q = 0$ ELF not only around valence and plasmon excitation features but also for low-energy excitations and for inner shell

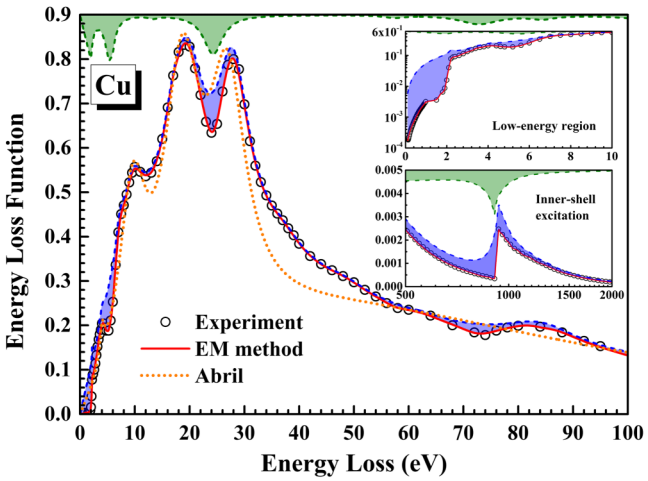

FIG. 1 (color online). Cu ELF in the optical limit ($q = 0$) as a function of excitation energy. Circles are experimental data [23–25]. The solid line represents the ELF fitted with the EM method, and dotted lines represent the ELF fitted from Abril *et al.* [17]. The blue and green lines represent the contribution of the negative oscillators. Insets show detail of the very low energy and inner shell excitation regions.

excitations at high energies. In addition, our method also naturally preserves two important sum rules when extended to infinite q values (see [26]).

Once the ELF is determined, the IMFP λ_{in} at an electron kinetic energy E can be calculated from

$$\lambda_{\text{in}}^{-1}(E) = \frac{\hbar}{\pi a_0 E} \int_0^{E-E_F} d\omega \int_{q_-}^{q_+} \text{Im}\left[\frac{-1}{\varepsilon(q,\omega)}\right] \frac{dq}{q}, \qquad (2)$$

where a_0 is the Bohr radius, E_F is the Fermi energy, and the integration limits, $\hbar q_\pm = (2m)^{1/2}[E^{1/2} \pm (E-\hbar\omega)^{1/2}]$, are the largest and smallest kinematically allowed momentum transfers for a given E and ω.

Figure 2 shows the IMFP for Cu from the EM method together with those from the previous approaches, along with experimental data from the EPES technique [7,8,27,28]. Open symbols represent IMFPs measured with traditional EPES from Tanuma *et al.* [7], Lesiak *et al.* [27], and Jablonski *et al.* [28]. Filled symbols show IMFPs from the improved EPES technique [8], which can provide more reliable results as a result of its independence from reference IMFP values. To verify the reliability of our method, we produced four separate IMFPs for Cu: from the ELF fitted using the EM method, from the NM-method fitted ELF [17], and from the full Penn algorithm (FPA) using both the original experimental data and the present fit, respectively. As we were able to avoid errors in the EM fitting procedure, it is quite reasonable to expect that the resulting IMFPs will differ only slightly from those calculated from the original experimental ELF. It is thus clear that the deviations in IMFPs calculated with the Mermin approach and the FPA must be due to the finite lifetimes of plasmons and other excitations that are considered in the Mermin approach. The use of Mermin terms in the q extension results in IMFPs that are smaller than those from the FPA over the whole energy range, and more than 25% lower at low energies (<200 eV). A detailed comparison of the FPA and Mermin approaches will be presented elsewhere.

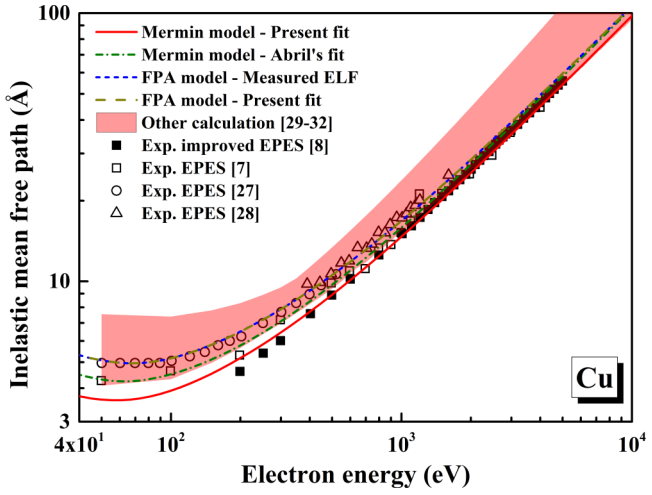

FIG. 2 (color online). Electron IMFPs as a function of electron energy for Cu. Filled symbols are experimental measurements from the improved EPES technique [8]. Open symbols are experimental data obtained with traditional EPES from Tanuma *et al.* (squares) [7], Lesiak *et al.* (circles) [27], and Jablonski *et al.* (triangles) [28]. Solid and dot-dashed lines represent IMFPs calculated with the EM method and our fitted ELF and with Abril *et al.*'s fitted ELF [17], respectively. Short-dashed and dashed lines show the IMFPs calculated with the FPA using the original experimental optical ELF and the EM-fitted ELF, respectively. The red band indicates the IMFPs predicted by other theoretical methods [29–32].

Note that the agreement between traditional EPES and calculated data from the FPA approach is due to the reference IMFP values employed in the traditional EPES measurements having been calculated *with* the FPA approach. It can be seen that the IMFP calculated from the EM method is in excellent agreement with the improved-EPES measurement [8] and lower than the data from traditional EPES [7,27,28]. The comparison with improved EPES confirms that the EM method provides better agreement than other theoretical predictions [29–32].

Turning to the theoretical methods' performance at low energy, Fig. 3 presents IMFPs from the EM method and XAFS-based experimental results [9] for Cu below 120 eV. We observe significant deviations of the IMFPs calculated with the Mermin model from the present fitted ELF and Abril *et al.*'s fit [17]. This discrepancy increases at first and then converges to a stable value about 15% lower than

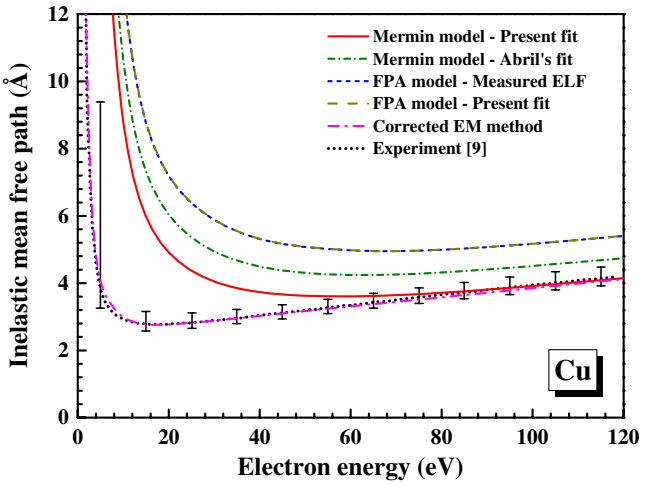

FIG. 3 (color online). Electron IMFPs as a function of electron energy for Cu at low energy. The dotted line shows the IMFP measured with the XAFS technique [9]. The solid, dot-short-dashed, short-dashed, and dashed lines show IMFPs calculated with the EM method with our fitted ELF and the Abril *et al.* fitted ELF [17], and by the FPA with the original experimental optical ELF and our fitted ELF, respectively. The dot-dashed line shows corrected results based on the EM method.

Abril *et al.*'s fit with increasing electron energy. These deviations mainly originate from small variations in ELFs in the infrared region and accumulate as electron energy increases [26]. The IMFPs predicted with our method show excellent agreement with the XAFS-based experimental data [9] between 50 and 120 eV. It is obviously that including Mermin oscillators in the infrared region is the key point for the EM method to reproduce experimental IMFP data at low energies. This is a strong validity of the (theoretical) EM method for determining IMFPs and also of the (experimental) XAFS technique. As a result of the unclear validation of the Born approximation, i.e., whether or not the screened electron-electron interaction is properly treated in lowest-order perturbation theory, our method persists in disagreeing strongly with the experimental data at very low energies, $\lesssim$40 eV. Although it is not clear whether the XAFS-based measurements or the present theoretical model dominates the discrepancy, we also found an interesting relationship between IMFPs determined by XAFS method and those of our EM method over 3–120 eV energy range. This relationship can be expressed by $\lambda_{\mathrm{XAFS}}/\lambda_M = 1 - \exp(-E/B)$, where λ_{XAFS} is IMFPs of XAFS method, λ_M is the IMFP result from the EM method, E is the electron kinetic energy, and B is a material-dependent parameter (i.e., $B_{\mathrm{Cu}} = 24$ eV, $B_{\mathrm{Mo}} = 26$ eV) which relevant to the compensation for the deviation of the Born approximation. The resulting corrected IMFPs λ_C that are calculated from $\lambda_C = \lambda_M[1 - \exp(-E/B_{\mathrm{Cu}})]$ are shown as dot-dashed line in Fig. 3. We see remarkable agreement between our corrected IMFPs and those of XAFS method over the whole energy range. Details of the discussions for parameter B will be presented elsewhere.

Figure 4 shows the resulting IMFPs for Mo from the EM approach together with XAFS measurements [10] (dotted line) in the energy range below 120 eV. The oscillator strengths a_i were again allowed to take negative values. The fitted ELF with the contributions from the positive and negative oscillators (blue and green lines) are shown in the inset. We employed 69 oscillators with 33 negative oscillators to fit the experimental optical ELF [25,33]. We produced IMFPs from the ELF fitted using the EM method, and from the FPA approach using the original experimental data and the present fit, respectively. The corrected IMFP results, with $B_{\mathrm{Mo}} = 26$ eV, are also shown. It is no surprise that the IMFPs calculated with the FPA using the present fit and using the experimental data are consistent, because of the accuracy of the EM method's ELF fit. The IMFPs calculated with the EM method are smaller than those from the FPA model as a consequence of the finite lifetimes of plasmons and other excitations considered in the Mermin approach. Agreement with experiment is significantly improved across the energy range shown, with the EM calculation being almost identical to the experimental data between 100 and 120 eV and nearly falling within the error bars at energies around 60 eV.

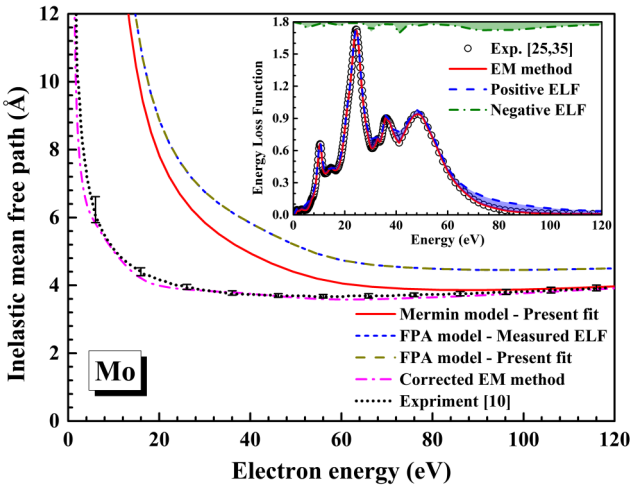

FIG. 4 (color online). Electron IMFPs as a function of electron energy for Mo at low energy. The solid, short-dashed, and dashed lines represent the IMFPs calculated with the EM method from our fitted ELF and with the FPA using the original experimental optical ELF and our fitted ELF, respectively. The dot-dashed line shows corrected results based on the EM method. The inset shows the Mo ELF fitted with the EM method (solid line). The blue and green lines indicate the contribution of negative oscillators. Symbols show the experimental optical ELF [25,33].

In summary, we have proposed an improved technique, dubbed the extended Mermin method, for determining IMFPs from measured optical ELFs. It is a more efficient election of the Mermin oscillators than the traditional Mermin method, especially in the infrared region. Taking infrared transitions into account, the resulting IMFPs for Cu and Mo are in excellent agreement with the most reliable experimental measurements, i.e., from the improved EPES technique on the high-energy side and from XAFS at low energies. This result is clear evidence that these excellent agreements with XAFS-based measurements in the region of 50–120 eV, where both the experimental and theoretical determinations should be considered most reliable, which is not produced by other theoretical models.

We thank Dr. C. J. Powell for helpful comments and discussions. Z. J. Ding acknowledges support from the National Natural Science Foundation of China (Grants No. 11274288 and No. 11204289) and the National Basic Research Program of China (Grants No. 2011CB932801 and No. 2012CB933702).

*DA.Bo@nims.go.jp
†Present address: Advanced Algorithm & Systems Co., 7F Ebisu-IS Building, 1-13-6 Ebisu, Shibuya, Tokyo 150-0013, Japan.

[1] *ISO18115 Surface Chemical Analysis—Vocabulary—Part 1: General terms and terms used in spectroscopy*

(International Organisation for Standardisation, Geneva, 2010).
[2] C. J. Powell and A. Jablonski, Nucl. Instrum. Methods Phys. Res., Sect. A **601**, 54 (2009).
[3] W. S. M. Werner, W. Smekal, H. Stori, H. Winter, G. Stefani, A. Ruocco, F. Offi, R. Gotter, A. Morgante, and F. Tommasini, Phys. Rev. Lett. **94**, 038302 (2005).
[4] D. P. Pappas, K.-P. Kamper, B. P. Miller, H. Hopster, D. E. Fowler, C. R. Brundle, A. C. Luntz, and Z.-X. Shen, Phys. Rev. Lett. **66**, 504 (1991).
[5] C. J. Powell and A. Jablonski, J. Phys. Chem. Ref. Data **28**, 19 (1999).
[6] G. Gergely, Prog. Surf. Sci. **71**, 31 (2002).
[7] S. Tanuma, T. Shiratori, T. Kimura, K. Goto, S. Ichimura, and C. J. Powell, Surf. Interface Anal. **37**, 833 (2005).
[8] S. Tanuma, H. Yoshikawa, N. Okamoto, and K. Goto, J. Surf. Anal. **15**, 195 (2008).
[9] J. D. Bourke and C. T. Chantler, Phys. Rev. Lett. **104**, 206601 (2010).
[10] C. T. Chantler and J. D. Bourke, J. Phys. Chem. Lett. **1**, 2422 (2010).
[11] J. D. Bourke, C. T. Chantler, and C. Witte, Phys. Lett. A **360**, 702 (2007).
[12] D. R. Penn, Phys. Rev. B **35**, 482 (1987).
[13] N. D. Mermin, Phys. Rev. B **1**, 2362 (1970).
[14] C. D. Denton, I. Abril, R. Garcia-Molina, J. C. Moreno-Marin, and S. Heredia-Avalos, Surf. Interface Anal. **40**, 1481 (2008).
[15] J. D. Bourke and C. T. Chantler, J. Phys. Chem. A **116**, 3202 (2012).
[16] C. T. Chantler and J. D. Bourke, J. Phys. Condens. Matter **26**, 145401 (2014).
[17] I. Abril, R. Garcia-Molina, C. D. Denton, F. J. Pérez-Pérez, and N. R. Arista, Phys. Rev. A **58**, 357 (1998).
[18] C. D. Denton, I. Abril, J. C. Moreno-Marín, S. Heredia-Avalos, and R. Garcia-Molina, Phys. Status Solidi (b) **245**, 1498 (2008).
[19] W. de la Cruz and F. Yubero, Surf. Interface Anal. **39**, 460 (2007).
[20] W. S. M. Werner, K. Glantsching, and C. A. Draxl, J. Phys. Chem. Ref. Data **38**, 1013 (2009).
[21] D. Tahir and S. Tougaard, J. Phys. Condens. Matter **24**, 175002 (2012).
[22] B. Da, Y. Sun, S. F. Mao, Z. M. Zhang, H. Jin, H. Yoshikawa, S. Tanuma, and Z. J. Ding, J. Appl. Phys. **113**, 214303 (2013).
[23] B. Dold and R. Mecke, Optik (Stuttgart) **22**, 435 (1965).
[24] H. J. Hagemann, W. Gudat, and C. Kunz, J. Opt. Soc. Am. **65**, 742 (1975).
[25] B. L. Henke, E. M. Gullikson, and J. C. Davis, At. Data Nucl. Data Tables **54**, 181 (1993).
[26] See Supplemental Material http://link.aps.org/supplemental/10.1103/PhysRevLett.113.063201, which includes Refs. [33–42].
[27] B. Lesiak, A. Jablonski, J. Zemek, and P. Jiricek, Surf. Interface Anal. **26**, 400 (1998).
[28] A. Jablonski and P. Jiricek, Surf. Sci. **412–413**, 42 (1998).
[29] J. M. Fernandez-Varea, F. Salvat, M. Dingfelder, and D. Liljequist, Nucl. Instrum. Methods Phys. Res., Sect. B **229**, 187 (2005).
[30] J. C. Ashley, J. Electron Spectrosc. Relat. Phenom. **46**, 199 (1988).
[31] C. J. Tung, J. C. Ashley, and R. H. Ritchie, Surf. Sci. **81**, 427 (1979).
[32] S. F. Mao, Y. G. Li, R. G. Zeng, and Z. J. Ding, J. Appl. Phys. **104**, 114907 (2008).
[33] E. D. Palik, *Handbook of Optical Constants of Solids* (Academic, New York, 1998).
[34] R. H. Ritchie and A. Howie, Philos. Mag. **36**, 463 (1977).
[35] J. C. Ashley, J. Electron Spectrosc. Relat. Phenom. **28**, 177 (1982).
[36] S. Tougaard and J. Kraaer, Phys. Rev. B **43**, 1651 (1991).
[37] D. J. Planes, R. Garcia-Molina, I. Abril, and N. R. Arista, J. Electron Spectrosc. Relat. Phenom. **82**, 23 (1996).
[38] R. Flitsch and S. I. Raider, J. Vac. Sci. Technol. **12**, 305 (1975).
[39] J. M. Hill, D. G. Royce, C. S. Fadley, L. F. Wagner, and F. J. Grunthaner, Chem. Phys. Lett., **44**, 225 (1976).
[40] R. Jung, J. C. Lee, G. T. Orosz, A. Sulyok, G. Zsolt, and M. Menyhard, Surf. Sci. **543**, 153 (2003).
[41] G. Gergely, S. Gurban, M. Menyhard, A. Jablonski, L. Zommer, and K. Goto, Vacuum **84**, 134 (2009).
[42] S. Heredia-Avalos, R. Garcia-Molina, J. M. Fernández-Varea, and I. Abril, Phys. Rev. A **72**, 052902 (2005).